Desalination behavior and performance of flow-electrode capacitive deionization under various operational modes

Kunyue Luo [a,b,1], Qiuya Niu [a,b,1], Yuan Zhu [a,b,1], Biao Song [a,b,1], Guangming Zeng [a,b,*], Wangwang Tang [a,b,*], Shujing Ye [a,b], Jing Zhang [a,b], Mengbiao Duan [a,b], Wenle Xing[a,b]

[a] College of Environmental Science and Engineering, Hunan University, Changsha 410082, China

[b] Key Laboratory of Environmental Biology and Pollution Control (Hunan University), Ministry of Education, Changsha 410082, China

*Corresponding authors: zgming@hnu.edu.cn (G. Zeng); wtang@hnu.edu.cn (W. Tang).

[1] These authors contribute equally to this article.

Abstract

Flow-electrode capacitive deionization (FCDI) has attracted growing attention due to its superior desalination capacity and continuous operation. This study, for the first time, systematically investigated the desalination behaviors of FCDI under a variety of operational modes and made a detailed comparison of relevant operation to provide useful information for selecting appropriate FCDI operational mode. Five operational modes with respect to the flow of electrodes and feed water were studied with both constant voltage and constant current applied. Results revealed that the effluent conductivity during charging decreased continuously in batch mode while decreased quickly and then leveled off in single-pass mode. pH of flow-electrodes fluctuated differently for the operational modes of isolated closed-cycle (ICC), short-circuited closed-cycle (SCC) and open cycle (OC), while pH of the effluent stream maintained stable for all operational modes. The variation of current or voltage could be explained by the change in the resistance of FCDI mainly induced by the middle-chamber salt concentration. Based on the three performance indicators of average salt removal rate, charge efficiency and removed salt normalized energy consumption, ICC/single-pass and SCC/single-pass are the two most superior operational modes, followed by OC/single-pass, ICC/batch-mode and SCC/batch-mode. Further considering the advantage of SCC in the continuous charge neutralization and electrode regeneration, SCC/single-pass operational mode can be deemed optimal.

Keywords: Flow-electrode capacitive deionization; Operational mode; Desalination

behavior; Desalination performance

1. Introduction

With the improvement of people's living standards and the rapid development of the economy, people's demand for clean water is continuously increasing. The shortage of freshwater resources has become one of the major problems facing many countries in the world [1, 2]. Seawater or brackish water desalination is conducive to increasing the freshwater supply beyond what is available from the hydrological cycle. As an electrochemical desalination technology, capacitive deionization (CDI) has received considerable attention in recent years due to its advantages of environmental friendliness (i.e., without the use of any additional chemicals or the generation of hazardous substances), low energy consumption (i.e., enabling ion removal at room temperatures, low pressures and low voltages with additional possibility of energy recovery), simple equipment structure, convenient process operation and facile electrode regeneration [3-5]. To date, CDI has progressed from its initial application of water desalination to the current applications in water purification, water disinfection, resource recovery, and synergistic combination with other technologies to achieve various ultimate goals [5-9].

CDI refers to the removal of ions using capacitive adsorption. When a limited potential difference (usually ≤ 1.23 V avoiding water hydrolysis) is applied, under the action of electric field force, cations and anions in solution flowing between a pair of porous carbon electrodes will move to the electrodes with opposite charge and

eventually stored in the electric double layers (EDLs) formed along the pore surfaces at the carbon/water interface, thereby producing a desalinated stream [4, 10]. When the electrodes are in short circuit or reversely connected, the adsorbed ions will be released to the bulk solution thereby producing a concentrated stream, and the electrodes are regenerated and regain their initial ion sorption capacity [11-13]. During ion electrosorption step in CDI, along with the counterion adsorption in EDLs, co-ions are expelled from electrode micropores and ultimately end up in the spacer channel and therefore reduce the desalination performance [10]. One important improvement over CDI is the inclusion of ion exchange membranes (IEMs) in front of the electrodes with this configuration called membrane capacitive deionization (MCDI) [14-17]. In MCDI, during charging, the co-ions expelled from the micropores are blocked by the IEMs and consequently accumulate in the macropores of the electrode, which increases the macropore co-ion concentration to the values beyond those in the spacer channel [18]. Due to the property of charge neutrality in the macropores, the electrode macropores of MCDI could serve as extra storage space for counterions, thereby improving charge efficiency and desalination performance [19, 20].

For (M)CDI systems, ion adsorption capacity is largely limited by the static electrodes, making (M)CDI only suitable for treating brackish/low-salinity water [14]. In addition, preparation of the fixed electrodes is kind of complicated and approximately 20% of the fabricated electrodes is made up of conductive agents (e.g., carbon black) and polymer binder (e.g., polytetrafluoroethylene) that have negligible

ion adsorption capacity [20, 21]. Furthermore, (M)CDI cells operate in an intermittent manner with the desalinated stream and brine stream produced alternately [22]. To solve these problems, flow-electrode capacitive deionization (FCDI) arising from the modification of MCDI through the use of flowing carbon materials instead of the fixed electrodes between current collectors and IEMs was recently developed and has attracted increasing attention [23-25]. FCDI delivers high salt removal efficiency for high-salinity water attributed to the infinite ion adsorption capacity of the flow-electrode based on the continuous inflow of uncharged carbon particles [26]. Moreover, the mobility of the electrodes allows regeneration of the electrode material external to the apparatus, thereby realizing continuous desalination and steady production of desalted water [27-29].

While optimizing the carbon materials and aqueous electrolyte constituting the flow-electrode and improving the FCDI cell design represent two main research efforts enhancing the desalination performance of FCDI [30-40], selecting a proper mode to effectively operate the FCDI system is also an important issue requiring consideration [32, 33]. Generally, with respect to the power aspect, there are two kinds of operational modes for the FCDI adsorption/desorption step, i.e., constant voltage and constant current [41]. In terms of fluid flow, there are three kinds of operational modes for flowing electrodes (isolated closed-cycle (ICC), short-circuited closed-cycle (SCC) and open cycle (OC)) and two kinds of operational modes for feed water (batch-mode and single-pass) [41-43]. As a result, there are twelve combinations of operational modes in total for a FCDI system. However, until now,

only a few of them have been investigated, such as constant voltage/ICC/batch-mode, constant voltage/SCC/batch-mode, constant voltage/SCC/single-pass, constant current/ICC/single-pass, and constant current/OC/single-pass [41-44]. Moreover, these reported operational modes were conducted in separate studies with very different experimental conditions, which makes it hard to compare the desalination behavior and desalination performance of FCDI under such scenarios. Therefore, in this work, we aimed at investigating the desalination behavior and performance of FCDI under the diverse range of operational modes, and making a detailed comparison of relevant FCDI operation to provide a reference for selecting an appropriate FCDI operational mode.

2. Materials and methods

2.1. FCDI cell configuration

The structure of the FCDI cell used in this study was shown in Figure 1. The graphite plate (150 mm × 80 mm × 6 mm) carved with serpentine flow channels that were 3 mm wide, 3 mm deep and 819 mm long from the inlet to the outlet was used as the current collector and the flow-electrode chamber. A nylon sheet (thickness of ~0.5 mm, 80 mesh, 150 mm × 80 mm) was put within the silicone gasket as the spacer channel enabling the feed water to flow through. The silicone gasket was used to prevent water leakage. A cation exchange membrane (CMI-7000, Membranes International Inc., USA) and an anion exchange membrane (AMI-7001, Membranes International Inc., USA) with the size of 182 mm × 112 mm × 0.45 mm were respectively placed between the graphite plate and the nylon spacer sheet. The

effective contact area between the flow electrode and the ion-exchange membrane was 24.6 cm^2. All the components were held together with the use of acrylic end plates (182 mm × 112 mm). Each of the acrylic end plates was engraved with a flat concave area of 150 mm × 80 mm with a depth of 6 mm for containing the graphite plate with the same dimension, with holes drilled around the perimeter of plates to allow for fastening with M3 bolts. Inlet and outlet ports were created using luer fittings. A stainless steel hex screw penetrated the middle of the acrylic plate to connect the graphite current collector with the anode or cathode of direct-current power supply.

Figure 1. Schematic of the structure of FCDI cell used in this work, which is similar to that in Ref. [45].

2.2. Experimental methods

The feed salt solution was prepared by dissolving analytical grade sodium chloride (NaCl) (Sigma Aldrich) in the deionized water (HHitech, China) in this study.

The flow electrode consists of 5 wt% activated carbon powder (No. 10006619, Sinopsin Chemical Reagent Co., Ltd., China), 1 wt% carbon black (LION Ketjenblack, ECP600JD, Japan) and 1 g/L NaCl solution. The specific surface area and average pore size of activated carbon power are 1449 m^2 g^{-1}, 2.78 nm, respectively, and the specific surface area and particle size of carbon black are 1400 m^2 g^{-1}, 0.048 nm, respectively. A direct-current power supply (MS155D, Maisheng Electronic Equipment Co., Ltd, China) was used to provide the required voltage or current. The dynamic voltage and current of the FCDI cell were recorded using a voltage probe (VP-BTA) and current probe (DCP-BTA) connected to a data acquisition system (SensorDAQ, Vernier, USA), respectively. The electrical conductivity and pH were monitored by the conductivity meter (DDS-307, INESA Scientific Instrument Co., Ltd, China) and pH meter (PHS-3C, INESA Scientific Instrument Co., Ltd, China), respectively. The flow rate of the feed water and the flow electrodes was controlled by peristaltic pumps (BT-300, Longer Precision Pump Co., Ltd, China). During the whole operation, no pH adjustment was carried out unless otherwise stated.

Five operational modes with respect to the flow of feed water and electrodes were chosen and tested under both constant current (4.06 A m^{-2}, 8.13 A m^{-2}, 12.16 A m^{-2}) and constant voltage (0.9 V, 1.2 V, 1.5 V): 1) The operational mode of ICC/batch-mode was displayed in Figure 2a. Slurry electrodes of 100 mL on each side were recirculated between the flow electrode chamber and the stirred vessels at a flow rate of 27 mL/min. 1 g/L NaCl solution (50 mL) was recirculated between the flow

channel and the stirred vessel at a flow rate of 11 mL/min. A 30-min constant-current (or constant-voltage) charging was followed by a 30-min equally reverse current (or voltage) discharging to regenerate the electrodes. 2) The operational mode of ICC/single-pass was displayed in Figure 2b. Slurry electrodes (100 mL each) were recirculated between the flow electrode chamber and the stirred vessels at a flow rate of 27 mL/min. 1 g/L NaCl solution as feedwater flowed through the middle chamber continuously at a flow rate of 11 mL/min without circulation. A 30-min constant-current (or constant-voltage) charging was followed by a 30-min equally reverse current (or voltage) discharging to regenerate the electrodes. The pH and conductivity of the desalinated water were measured at the outlet of FCDI cell. 3) The operational mode of SCC/batch-mode was displayed in Figure 2c. 200 mL slurry electrode in one stirred reservoir was pumped at a total flow rate of 54 mL/min in parallel through the anodic and cathodic flow channels and then returned and mixed in the reservoir with this approach resulting in charge neutralization and regeneration of the electrodes. The feed salt water made of 1 g/L NaCl (50 mL) was recycled at a flow rate of 11 mL/min. 4) The operational mode of SCC/single-pass was displayed in Figure 2d. 200 mL slurry electrode in one stirred reservoir was pumped at a total flow rate of 54 mL/min in parallel through the anodic and cathodic flow channels and then returned and mixed in the reservoir. The feed salt water made of 1 g/L NaCl continuously flowed through the middle chamber at a flow rate of 11 mL/min without circulation. 5) The operational mode of OC/single-pass was displayed in Figure 2e. Fresh slurry electrode on each side was pumped through the flow-electrode chamber

continuously at a flow rate of 27 mL/min without circulation. The feed salt water made of 1 g/L NaCl continuously flowed through the middle chamber at a flow rate of 11 mL/min without circulation.

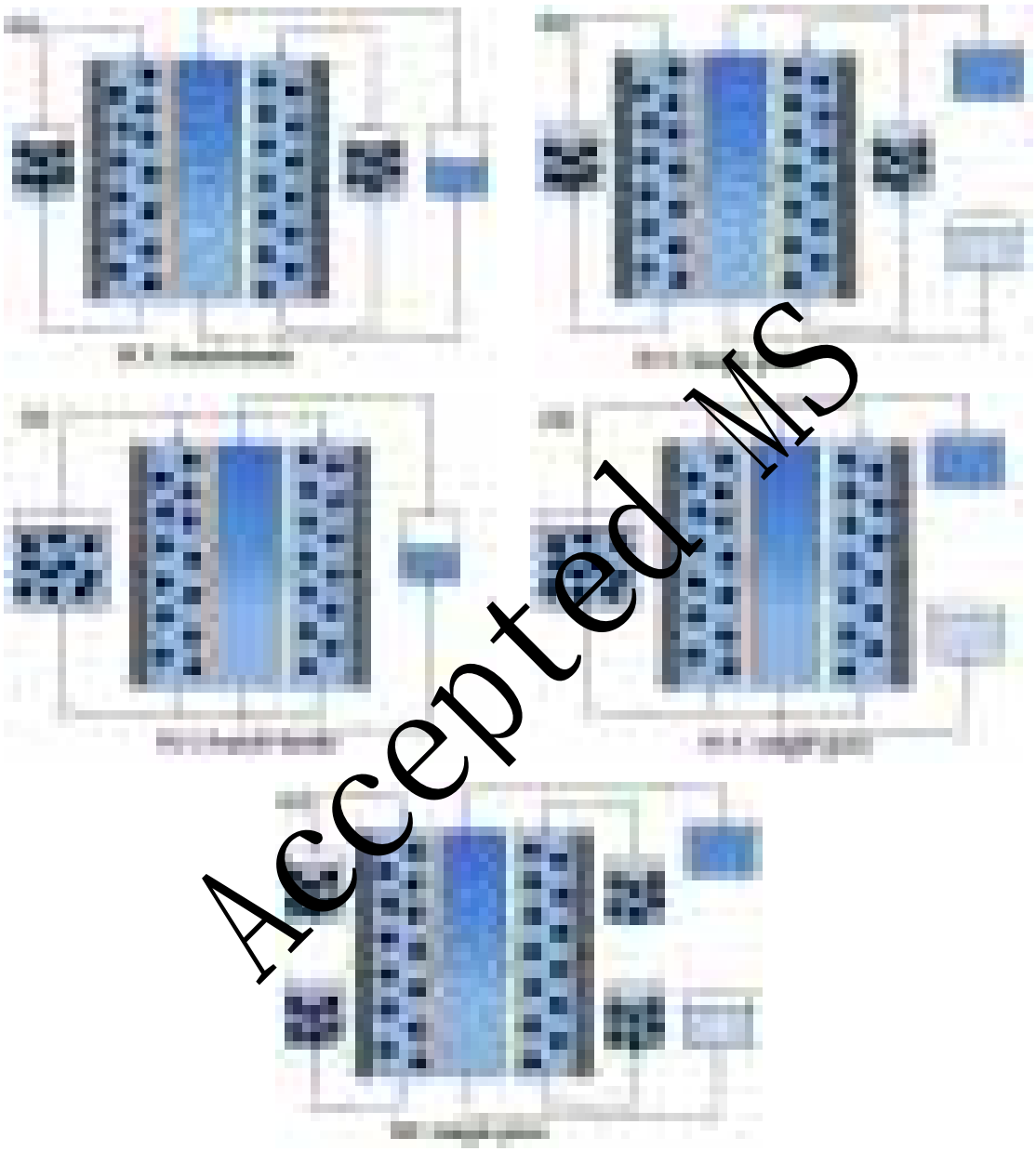

Figure 2. Operational modes of the (a) ICC/batch-mode, (b) ICC/single-pass, (c) SCC/batch-mode, (d) SCC/single-pass, and (e) OC/single-pass for FCDI system with regard to flow of feed water and electrodes.

Conductivity data were converted to NaCl concentration using the calibration

curve shown in Figure S1. The amount of removed salt Q (mmol) during charging in batch-mode and single-pass mode can be respectively calculated with the equations below :

$$Q = \frac{(c_o - c_i) \times V}{M} \quad (1)$$

$$Q = \frac{v \times \int_0^T (C_0 - C_i) dt}{M} \quad (2)$$

where C_0 (mg/L) is the initial NaCl concentration of the feed water, C_i (mg/L) is the NaCl concentration of the effluent at time i; V (L) is the volume of the treated water; v (L/s) is the flow rate of the feed water; M (g/mol) is the molar mass of NaCl; and T (s) is the charging time (1800 s).

The average salt removal rate (ASRR, mmol cm^{-2} min^{-1}) was calculated according to the following equation:

$$\mathrm{ASRR} = \frac{Q}{A_{\mathrm{eff}} \cdot T} \quad (3)$$

where A_{eff} is the effective contact area between the flow electrode and the ion-exchange membrane (24.6 cm^2).

The charge efficiency (λ) was calculated according to the following equation:

$$\lambda(\%) = \frac{F \times Q}{1000 \times \int_0^T I \cdot A_{\mathrm{eff}} \cdot dt} \times 100 \quad (4)$$

where F is the Faraday's constant, 96485 C/mol; I is current density, A m^{-2}.

The removed salt normalized energy consumption (RSNEC, J/mmol) under constant-voltage and constant-current operation during charging were given by

$$\mathrm{RSNEC_{cv}} = \frac{V_{\mathrm{cv}} \times \int_0^T I \cdot A_{\mathrm{eff}} dt}{Q} \quad (5)$$

$$\mathrm{RSNEC_{cc}} = \frac{I_{\mathrm{cc}} \times A_{\mathrm{eff}} \times \int_0^T V dt}{Q} \quad (6)$$

where V_{cv} (V) represents the applied constant voltage, I_{cc} (A m^{-2}) represents the

applied constant current density; V (V) and I (A m^{-2}) represent the voltage across and the current density through the FCDI electrodes, respectively.

3. Results and discussion

3.1. Desalination behavior of FCDI under various operational modes

3.1.1. Operational mode of ICC/batch-mode

Figure 3a shows the temporal variation of effluent conductivity of FCDI in the operational mode of ICC/batch-mode with a constant voltage or constant current applied. In this mode, after 30 min constant-voltage (or constant-current) charging, an equally reversed constant-voltage (or constant-current) was applied for 30 min discharging (desorption and electrode regeneration). As can be seen, during charging, a constant current led to a steady decrease in the effluent conductivity with the salt ions being continuously removed from the middle desalination chamber, and a higher constant current contributed to a more rapid decline. At a constant current density of 4.06 A m^{-2}, 8.13 A m^{-2}, 12.16 A m^{-2}, the effluent conductivity decreased from 1758 μs cm^{-1} to 1295 μs cm^{-1}, 1051 μs cm^{-1}, 740 μs cm^{-1}, respectively. In the discharging stage, under the constant-current operation, the effluent conductivity steadily increased, finally returning back to the initial value of feed water. The effluent conductivity under constant-voltage operation exhibited similar trends to that under constant-current operation except for the desorption step. Under constant-voltage operation, the effluent conductivity during discharging increased more quickly, and after 30-min running, it exceeded the initial value of feed water with a higher voltage leading to a greater discrepancy. This implied that some additional ions originally in

the flow electrodes passed through the ion-exchange membranes entering the middle desalination chamber noting that we prepared the flow electrodes using 1 g/L NaCl electrolyte.

Figure 3b shows the temporal variation of pH in the positively and negatively charged flow-electrode chambers. Gradual pH increase (production of OH^-) was observed in the flow-cathode chamber while gradual pH decrease (production of H^+) was observed in the flow-anode chamber during charging with a larger constant-current or constant-voltage resulting in a greater pH excursion. It has been reported that the pH increase during electrochemical desalination in the cathode chamber can be attributed to the occurrence of oxygen reduction and/or hydrogen evolution, while the acidification in the anode chamber may be ascribed to the oxidation of the graphite and chloride and/or splitting of water [33, 36]. These redox reactions become less significant at a lower charging voltage or current, and therefore lead to less significant pH change. Charge neutralization in the flow electrodes reveals that certain amounts of Na^+ and Cl^- ions were not adsorbed in the carbon particles but were rather equilibrated OH^- and H^+ ions in the aqueous phase of the flow-electrodes, which underlines an additional electrodialytical desalination mechanism proceeding in parallel to the known electrosorption mechanism. During the regeneration of flow-electrodes by polarity reversal, reverse pH variations were observed, which can be explained by reversible Faradaic formations of H^+ and OH^- ions on the anode and cathode, respectively. The pH variation in the middle desalination chamber during charging and discharging cycles was displayed in Figure S3a. The pH of the effluent

stream maintained stable suggesting that symmetric removal (or release) of anions and cations (including H^+ and OH^-) from (or into) the brackish stream took place.

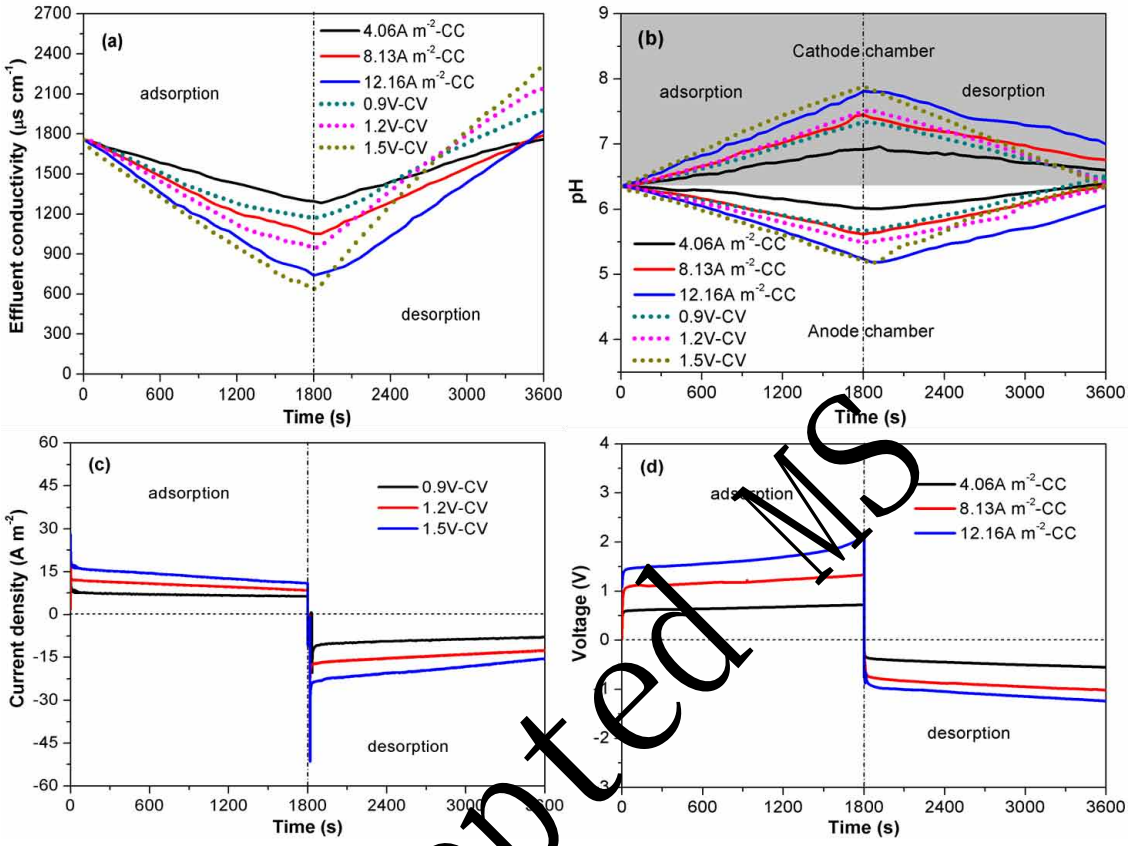

Figure 3. Temporal variation of (a) effluent conductivity, (b) pH in flow-electrode chambers, (c) current through the FCDI and (d) voltage between the FCDI performed under constant current and constant voltage for the operational mode of ICC/batch-mode.

Figures 3c and 3d respectively show the dynamic variation of current through the FCDI performed under constant voltage and the voltage between the FCDI performed under constant current. When the FCDI system was operated under constant voltage, the electrical current initially dropped quickly and then decreased slowly during charging with a higher constant voltage leading to a larger current. On reversing the polarity, the changing trend of the absolute value of current was quite similar to that during charging. When the FCDI system was operated under constant current, the cell

voltage rose to a certain point very quickly at the beginning (with a larger current corresponding to a higher starting point) and then gradually increased. For a low constant current (say, 4.06 A m^{-2}), the increase amplitude was very small and could be negligible within 30 min charging. For a large constant current (say, 12.16 A m^{-2}), the voltage increased slowly in the early stage but rose rapidly in the later period of charging. On reversing the polarity, the cell voltage suddenly turned negative and gradually decreased.

3.1.2. Operational mode of ICC/single-pass

Figure 4a presents the dynamic change of conductivity of the desalted water in the operational mode of ICC/single-pass with a constant voltage or constant current applied. It is observed that different from the profile in batch mode that the effluent conductivity continuously decreased, the effluent conductivity in single-pass mode decreased quickly and then leveled off after the commencement of the adsorption. Once the regeneration of flow-electrodes began, the effluent conductivity increased sharply followed by a relatively stable level. In addition, when the other parameters were fixed, upon increasing the current or voltage, the steady-state effluent conductivity decreased during adsorption. These findings reveal significant environmental implication that, in the ICC mode, treating the feed salt water in single-pass could produce an effluent stream with stable and adjustable ion concentrations. The temporal variations of pH in the positively and negatively charged flow-electrode chambers, pH of the effluent stream, the current through the FCDI and the voltage between the FCDI performed under either constant current or

constant voltage in the operational mode of ICC/single-pass were similar to those in the operational mode of ICC/batch-mode (see Figures 4 and S3b). One exception is the variation of voltage during charging at the constant current density of 12.16 A m^{-2}. In ICC/batch-mode, the voltage increased slowly in the early stage but rose rapidly in the later period of charging, whereas, in ICC/single-pass mode, the voltage increased slowly throughout the charging period. This could be explained by the significant difference in the salt concentration of the middle chamber. In ICC/batch-mode, the low salt concentration of the middle chamber in the later period of charging resulted in a rapid increase in the electrical resistance of the middle chamber. By contrast, the salt concentration of the middle chamber in ICC/single-pass mode remained stable, which implies a stable electrical resistance of the middle chamber.

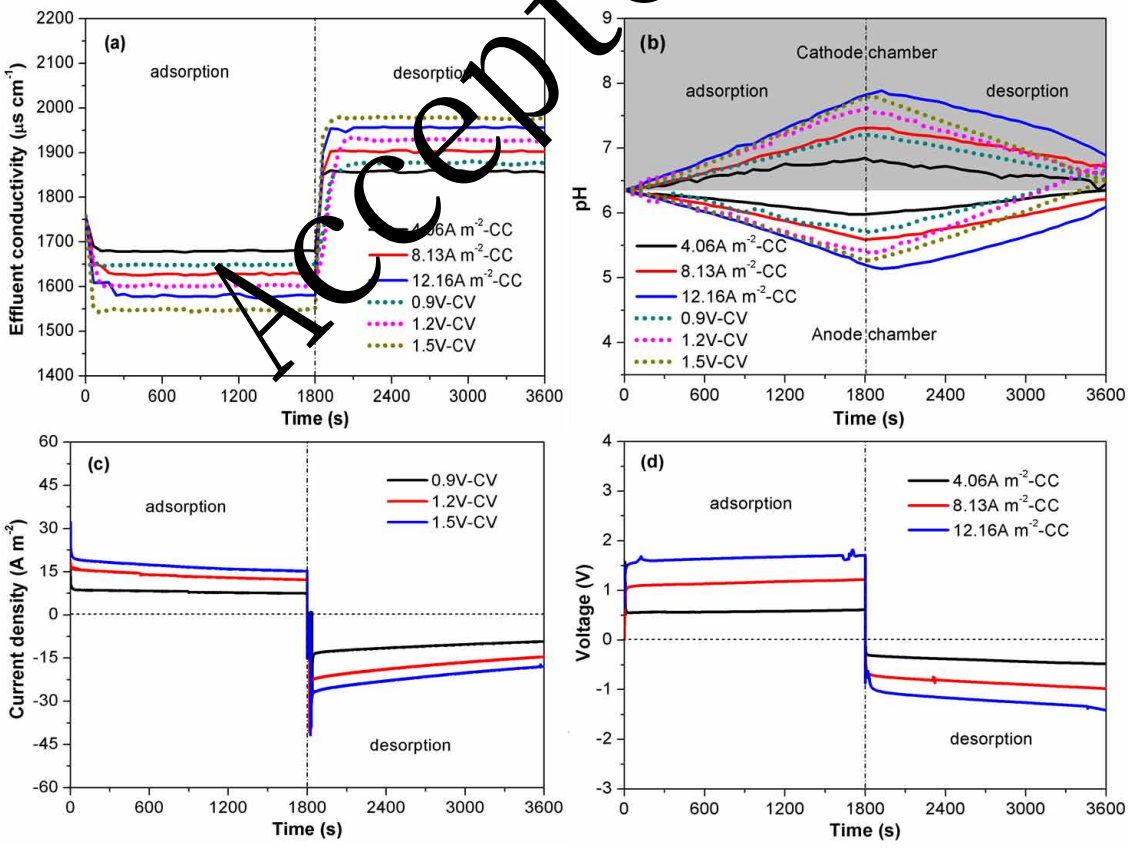

Figure 4. Temporal variation of (a) effluent conductivity, (b) pH in flow-electrode chambers, (c)

current through the FCDI, and (d) voltage between the FCDI performed under constant current and constant voltage for the operational mode of ICC/single-pass.

3.1.3. Operational mode of SCC/batch-mode

Figure 5a shows the change of effluent conductivity in the operational mode of SCC/batch-mode with a constant voltage or constant current applied. Note that SCC does not require a discharging step as charge neutralization of the flow-electrodes and regeneration of the carbon particles occur in the mixing reservoir. Therefore, we kept running the adsorption process for 1 hour. It can be observed that the effluent conductivity (i.e., effluent salt concentration) steadily decreased with the application of a constant voltage/constant current, and when the effluent conductivity dropped to a low value (say, 200 μs cm^{-1}) induced by a large voltage/current, the decreasing rate began to slow down. According to the recorded data of current/voltage variation in Figures 5c and 5d, it can be known that there was a positive correlation between the decreasing rate of effluent conductivity and the current density. At a constant-voltage charging of 0.9 V, the current through the FCDI remained unchanged, and the effluent conductivity declined at a fixed rate. Enhancing the charging voltage to 1.2 V and 1.5 V led to a decrease in the current at the later period which corresponded to a reduced decline rate in effluent conductivity. The decrease of current was largely due to the increase in the electrical resistance of middle chamber caused by the resulting low salt concentration. The variation of voltage under constant-current charging could be also explained by the change in the resistance of FCDI mainly induced by the middle-chamber salt concentration. Here, it should be noted that we set the maximum

cell voltage to be 3 V. Therefore, at a constant-current charging of 12.16 A m^{-2}, the voltage kept constant after it reached 3 V which, in fact, should grow exponentially without control.

Fluctuations in pH values in the effluent stream and in the flow electrode were also monitored for the operational mode of SCC/batch-mode. As expected, the variation of pH of the effluent was insignificant as presented in Figure S3c. The pH value of the electrode slurry also changed slightly since acid-base neutralization occurred as a result of mixing of the flow-electrodes.

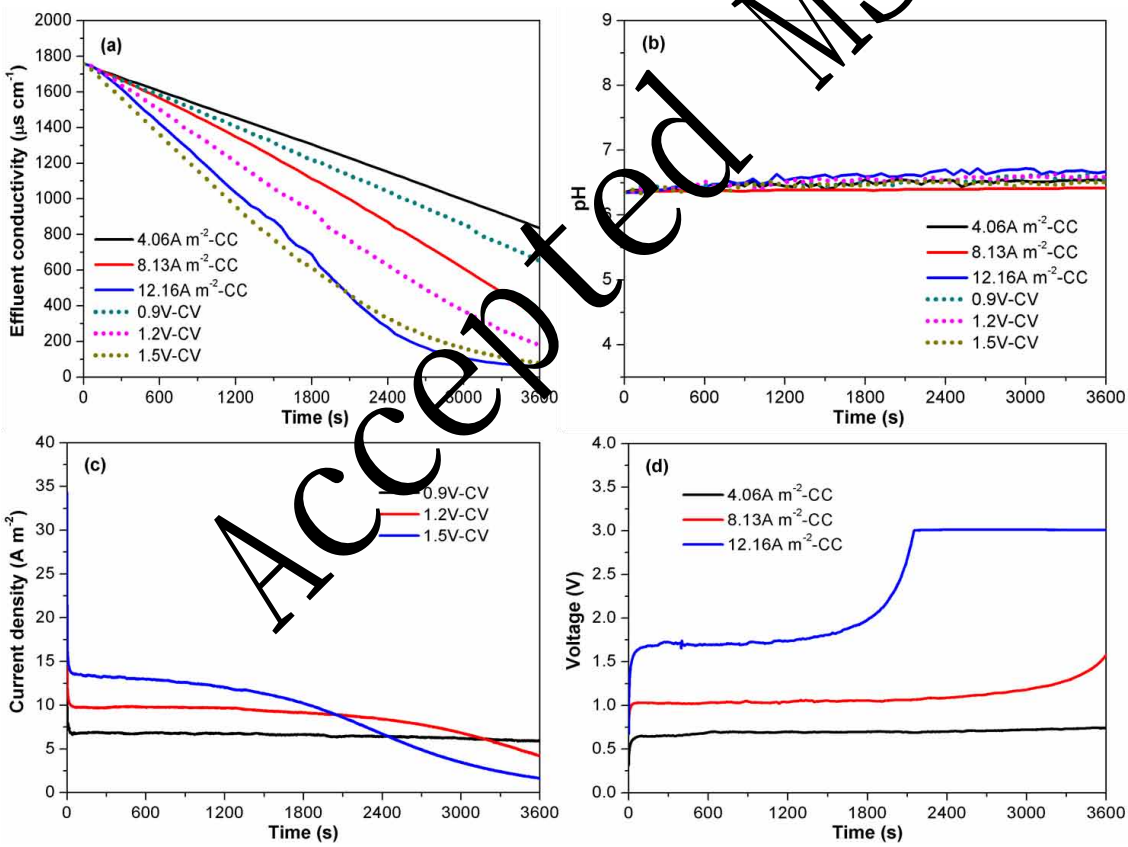

Figure 5. Temporal variation of (a) effluent conductivity, (b) pH in flow-electrode chambers, (c) current through the FCDI, and (d) voltage between the FCDI performed under constant current and constant voltage for the operational mode of SCC/batch-mode.

3.1.4. Operational mode of SCC/single-pass

Figure 6 shows the change of effluent conductivity, pH of the flow electrode, the current through the FCDI and the voltage between the FCDI in the operational mode of SCC/single-pass with a constant voltage or constant current applied. Similar to SCC/batch-mode, there was no desorption stage in SCC/single-pass because of the mixing and automatic regeneration of the carbon particles. In SCC/single-pass mode, upon applying a constant current or voltage, the effluent conductivity decreased rapidly and afterward reached a steady state exhibiting stable values. A larger constant current or constant voltage contributed to a lower steady-state effluent conductivity and hence a greater salt removal efficiency. The insignificant variation in current under constant-voltage charging and the insignificant variation in voltage under constant-current charging (Figure 6c and 6d) both revealed that the electrical resistance of the FCDI system kept basically constant, which was in accordance with the steady-state effluent conductivity in the middle spacer chamber. Since the anode electrode slurry and cathode electrode slurry mixed in a reservoir in SCC operation, the pH excursion was significantly inhibited in the flow electrode, as shown in Figure 6b. The fluctuation of pH in the effluent was also not obvious as expected (see Figure S3d).

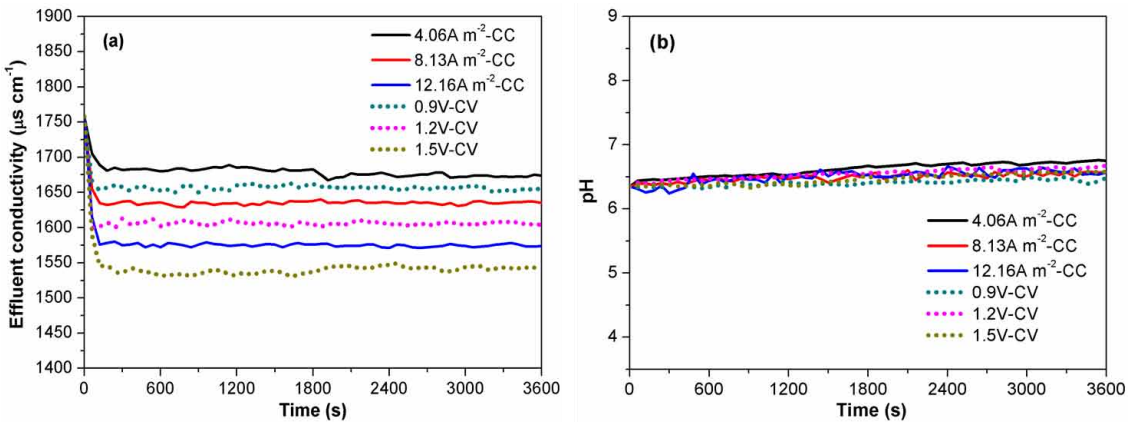

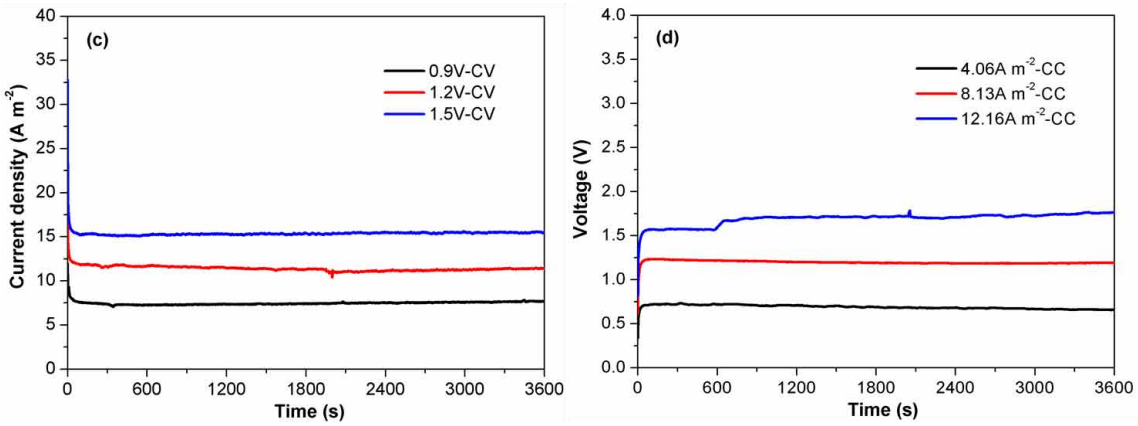

Figure 6. Temporal variation of (a) effluent conductivity, (b) pH in flow-electrode chambers, (c) current through the FCDI, and (d) voltage between the FCDI performed under constant current and constant voltage for the operational mode of SCC/single-pass.

3.1.5. Operational mode of OC/single-pass

Figure 7 shows the change of effluent conductivity, pH of the flow anode and cathode, the current through the FCDI and the voltage between the FCDI in the operational mode of OC/single-pass with a constant voltage or constant current applied. The profile of effluent conductivity versus time in OC/single-pass was similar to the others operated in single-pass mode, i.e., a rapid decrease in conductivity at the beginning followed by a steady-state change with a larger constant current or constant voltage contributing to a lower steady-state effluent conductivity. However, it should be noted that, under the same constant current or constant voltage, the steady-state effluent conductivity in OC/single-pass appeared to be a little higher than those in ICC/single-pass and SCC/single-pass, implying that OC/single-pass was kind of less effective in removing salt from the middle spacer chamber compared to ICC/single-pass and SCC/single-pass. From Figure 7b, it can be observed that, in OC/single-pass, the pH of the anodic flow electrode decreased slightly and then

stabilized, while the pH of the cathodic flow electrode increased slightly and then stabilized. This is because H^+ was produced in the anode chamber where the oxidation of the graphite and chloride and/or splitting of water were likely to occur and OH^- was produced in the cathode chamber where the oxygen reduction and/or hydrogen evolution probably occurred. And since the flow electrodes passed through the electrode chamber only once instead of recirculating, the pH fluctuations of flow anode and cathode were considered small, which was quite different from the pH variation in ICC/single-pass where pH continuously increased or decreased during charging due to the accumulation of OH^- or H^+. In Figures 7c and 7d, the profile of current under constant-voltage charging and the profile of voltage under constant-current charging could be explained by the change of resistance of the FCDI system which could be further explained by the variation of effluent conductivity [24, 33]. For example, the decrease in conductivity led to an increased resistance and the steady-state conductivity led to a stable resistance.

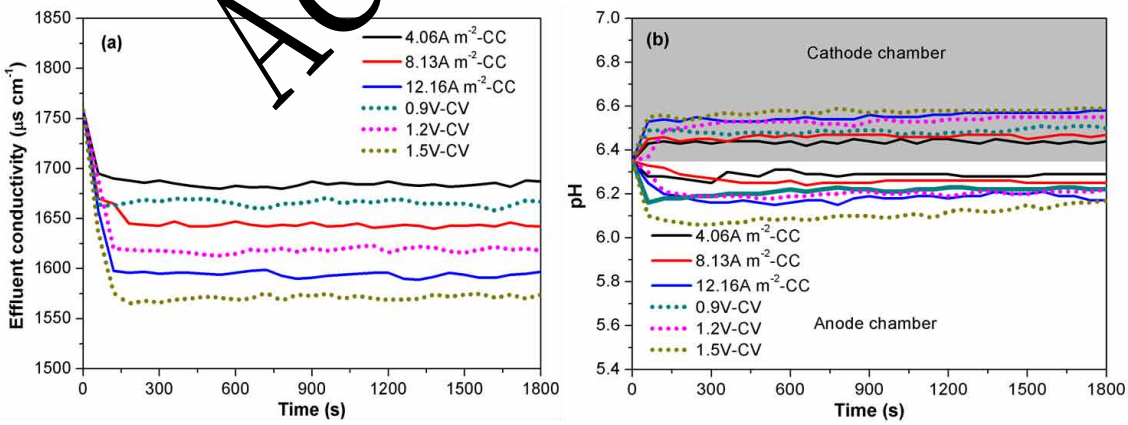

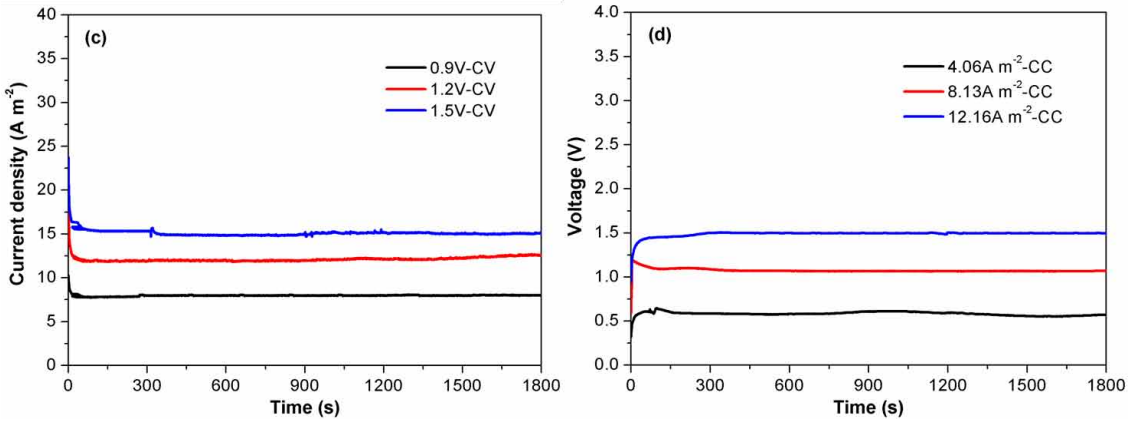

Figure 7. Temporal variation of (a) effluent conductivity, (b) pH in flow-electrode chambers, (c) current through the FCDI, and (d) voltage between the FCDI performed under constant current and constant voltage for the operational mode of OC/single-pass.

3.2. Desalination performance of FCDI under various operational modes

In FCDI, ion removal can be attributed to electrosorption and electrodialysis, and therefore, average salt removal rate (ASRR) is more appropriate than average salt adsorption rate (ASRR) to evaluate the desalination performance. When calculating ASRR, we unified the charging time to be 30 min so that ASRR was comparable under different operational modes. We can compare the changes in the CV mode and CC mode in addition to the ASRR under different operational modes. From Figure 8, we can see that ASRR increased with the increase in the applied charging voltage or current for any of the examined operational modes. The highest ASRR was obtained in the operational modes of ICC/single-pass and SCC/single-pass, which was followed by the operational modes of OC/single-pass, ICC/batch-mode and SCC/batch-mode. Overall, the ASRR under single-pass operating mode was larger than that under batch-mode operating mode though the difference was not that significant.

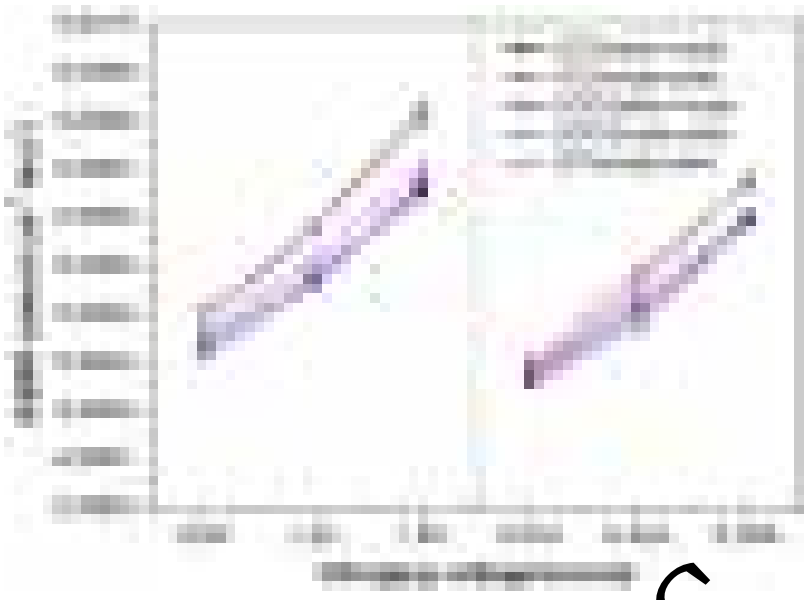

Figure 8. Average salt removal rate of the FCDI cell under different operational modes with constant voltage or constant current applied.

As shown in Figure 9, generally, the charge efficiency decreased with the charging voltage increasing from 0.9 V to 1.5 V or with the charging current increasing from 0.01 A to 0.03 A. This is because, at higher charging voltage or current, Faradaic reactions would occur more intensively thereby leading to a reduced charge efficiency [35, 46-47]. In addition, it was observed that, for different operational modes, the charge efficiency from high to low had the following order: ICC/single-pass, SCC/single-pass, OC/single-pass, ICC/batch-mode and SCC/batch-mode. The charge efficiency in single-pass mode was higher than that in batch-mode and this could be explained by the fact that, in single-pass mode, feed salt water with a constant NaCl concentration continuously flowed into the FCDI cell and more ions existed in the middle desalination chamber which enabled a larger amount of ions to pass through the IEMs and be adsorbed by the charged flow-electrodes. Also of note is that, under either single-pass mode or batch-mode, the charge

efficiency of ICC was the highest, which was followed by SCC and OC. This could be explained by the following scientific reasoning: imagining that one electron transferred from the current collector to the carbon particle in the flow-cathode, this electron would finally play a role by adsorbing one Na^+ ion through the continuous recycling of the flow-cathode electrodes (i.e., ICC mode). However, for OC mode, the carbon particle carrying this electron might leave the FCDI cell before functioning to adsorb the Na^+ ion consequently resulting in a loss of charge. The situation of SCC mode fell in between the ICC mode and OC mode.

Figure 9. Charge efficiency of the FCDI cell under (a) constant voltage and (b) constant current for different operational modes.

Energy consumption is another important indicator to evaluate the FCDI performance when FCDI is operated under different modes. For the ease of comparison, the values were normalized by the salt adsorption capacity (J/mmol). Figure 10 shows the removed salt normalized energy consumption (RSNEC) of FCDI under different operational modes with constant voltage or constant current applied, from which we can see that, whether in constant-voltage mode or constant-current mode, ICC/single-pass and SCC/single-pass operational modes were similar in energy

consumption. The energy consumption of OC/single-pass, ICC/batch-mode and SCC/batch-mode were higher than that of ICC/single-pass and SCC/single-pass. To sum up, ICC/single-pass and SCC/single-pass are the two best operational modes according to the three performance indicators of average salt removal rate, charge efficiency and removed salt normalized energy consumption. Further considering the advantage of SCC operation in the continuous charge neutralization and electrode regeneration that maintains pseudo infinite capacity during electrosorption, it can be concluded that SCC/single-pass operational mode is optimal.

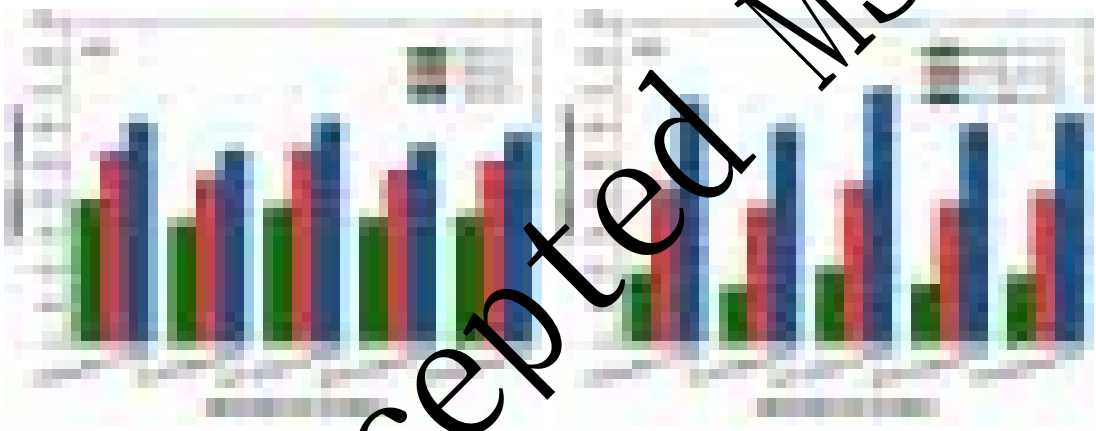

Figure 10. The removed salt normalized energy consumption (RSNEC) of FCDI under different operational modes with (a) constant voltage or (b) constant current applied.

4. Conclusions

In this study, the desalination behavior and performance of FCDI under various operational modes were examined. Experimental results indicated that the effluent conductivity during charging operated in batch-mode decreased continuously while effluent conductivity in single-pass mode decreased quickly and then leveled off with the application of a constant voltage/current. For ICC operation, gradual pH increase was observed in the flow-cathode chamber while gradual pH decrease was observed

in the flow-anode chamber during charging with a larger constant-current or constant-voltage resulting in a greater pH excursion. For SCC operation, pH of the electrode slurry changed slightly since acid-base neutralization occurred as a result of mixing of the flow-electrodes. For OC operation, the pH of the anodic flow electrode decreased slightly and then stabilized, while the pH of the cathodic flow electrode increased slightly and then stabilized. The pH of the effluent stream maintained stable for all kinds of operational modes. The decrease of current under constant-voltage charging was largely due to the increase in the electrical resistance of middle desalination chamber caused by the resulting low salt concentration. The variation of voltage under constant-current charging could be also explained by the change in the resistance of FCDI mainly induced by the middle-chamber salt concentration. ICC/single-pass and SCC/single-pass are the two most superior operational modes, followed by OC/single-pass, ICC/batch-mode and SCC/batch-mode, based on the performance indicators of average salt removal rate, charge efficiency and removed salt normalized energy consumption. SCC operation has additional advantages of the continuous charge neutralization and electrode regeneration that maintains pseudo infinite capacity during electrosorption. The OC operation requires preparation of more electrode materials, which is considered unadvisable for economic reasons. Single-pass mode is suitable for the requirement of constant effluent salt concentration.

Declaration of interest

The authors declare no competing financial interest.

Acknowledgements

This study was financially supported by the National Natural Science Foundation of China (51809088, 51521006), Huxiang High-Level Talent Gathering Project of Hunan Province (2019RS1025), the Fundamental Research Funds for the Central Universities (531118010106) and the Three Gorges Follow-up Research Project (2017HXXY-05).

References

[1] T.A. Larsen, S. Hoffmann, C. Lüthi, B. Truffer, M. Maurer, Emerging solutions to the water challenges of an urbanizing world, Science 352 (2016) 928-933.

[2] M. Elimelech, W.A. Phillip, The future of seawater desalination: energy, technology, and the environment, Science 333 (2011) 712-717.

[3] N. Ghaffour, T.M. Missimer, G.L. Amy, Technical review and evaluation of the economics of water desalination: Current and future challenges for better water supply sustainability, Desalination 309 (2013) 197-207.

[4] S. Porada, R. Zhao, A. van der Wal, V. Presser, P.M. Biesheuvel, Review on the science and technology of water desalination by capacitive deionization, Prog. Mater. Sci. 58 (2013) 1388-1442.

[5] M.E. Suss, S. Porada, X. Sun, P.M. Biesheuvel, J. Yoon, V. Presser, Water desalination via capacitive deionization: what is it and what can we expect from it? Energy Environ. Sci. 8 (2015) 2296-2319.

[6] W. Tang, J. Liang, D. He, J. Gong, L. Tang, Z. Liu, D. Wang, G. Zeng, Various cell architectures of capacitive deionization: Recent advances and future trends, Water Res. 150 (2019) 225-251.

[7] K. Fang, H. Gong, W. He, F. Peng, C. He, K. Wang, Recovering ammonia from municipal wastewater by flow-electrode capacitive deionization, Chem. Eng. J. 348 (2018) 301-309.

[8] O. Pastushok, F. Zhao, D.L. Ramasamy, M. Sillanpää, Nitrate removal and recovery by capacitive deionization (CDI), Chem. Eng. J. 375 (2019) 121943.

[9] K. Tang, Y.-h. Kim, J. Chang, R.T. Mayes, J. Gabitto, S. Yiacoumi, C. Tsouris, Seawater desalination by over-potential membrane capacitive deionization: Opportunities and hurdles, Chem. Eng. J. 357 (2019) 103-111.

[10] M.A. Anderson, A.L. Cudero, J. Palma, Capacitive deionization as an electrochemical means of saving energy and delivering clean water. Comparison to present desalination practices: Will it compete? Electrochim. Acta 55 (2010) 3845-3856.

[11] W. Xing, J. Liang, W. Tang, G. Zeng, X. Wang, X. Li, L. Jiang, Y. Luo, X. Li, N. Tang, M. Huang, Perchlorate removal from brackish water by capacitive deionization: Experimental and theoretical investigations, Chem. Eng. J. 361 (2019) 209-218.

[12] H. Li, L. Pan, T. Lu, Y. Zhan, C. Nie, Z. Sun, A comparative study on electrosorptive behavior of carbon nanotubes and graphene for capacitive deionization, J. Electroanal. Chem. 653 (2011) 40-44.

[13] W. Tang, X. Wang, G. Zeng, J. Liang, X. Li, W. Xing, D. He, L. Tang, Z. Liu, Electro-assisted adsorption of Zn(II) on activated carbon cloth in Bbatch-flow mode: experimental and theoretical investigations, Environ. Sci. Technol. 53 (2019) 2670-2678.

[14] R. Zhao, S. Porada, P.M. Biesheuvel, A. van der Wal, Energy consumption in membrane capacitive deionization for different water recoveries and flow rates, and comparison with reverse osmosis, Desalination 330 (2013) 35-41.

[15] C. Tan, C. He, W. Tang, P. Kovalsky, J. Fletcher, T.D. Waite, Integration of photovoltaic energy supply with membrane capacitive deionization (MCDI) for salt removal from brackish waters, Water Res. 147 (2018) 276-286.

[16] W. Tang, D. He, C. Zhang, T.D. Waite, Optimization of sulfate removal from brackish water by membrane capacitive deionization (MCDI), Water Res. 121 (2017) 302-310.

[17] J. Chang, K. Tang, H. Cao, Z. Zhao, C. Su, Y. Li, F. Duan, Y. Sheng, Application of anion exchange membrane and the effect of its properties on asymmetric membrane capacitive deionization,

Sep. Purif. Technol. 207 (2018) 387-395.
[18] J.-H. Lee, J.-H. Choi, The production of ultrapure water by membrane capacitive deionization (MCDI) technology, J. Membrane Sci. 409-410 (2012) 251-256.
[19] A. Rommerskirchen, B. Ohs, K.A. Hepp, R. Femmer, M. Wessling, Modeling continuous flow-electrode capacitive deionization processes with ion-exchange membranes, J. Membrane Sci. 546 (2018) 188-196.
[20] S. Wang, G. Wang, T. Wu, C. Li, Y. Wang, X. Pan, F. Zhan, Y. Zhang, S. Wang, J. Qiu, Membrane-free hybrid capacitive deionization system based on redox reaction for high-efficiency NaCl removal, Environ. Sci. Technol. 53 (2019) 6292-6301.
[21] S. Wang, G. Wang, T. Wu, Y. Zhang, F. Zhan, Y. Wang, J. Wang, Y. Fu, J. Qiu, BCN nanosheets templated by g-C 3 N 4 for high performance capacitive deionization, J. Mater. Chem. A 6 (2018) 14644-14650.
[22] Y. Bian, X. Yang, P. Liang, Y. Jiang, C. Zhang, X. Huang, Enhanced desalination performance of membrane capacitive deionization cells by packing the flow chamber with granular activated carbon, Water Res. 85 (2015) 371-376.
[23] S.-i. Jeon, H.-r. Park, J.-g. Yeo, S. Yang, C.H. Cho, M.H. Han, D.K. Kim, Desalination via a new membrane capacitive deionization process utilizing flow-electrodes, Energy Environ. Sci. 6 (2013) 1471.
[24] S. Yang, J. Choi, J.G. Yeo, S.I. Jeon, H.R. Park, D.K. Kim, Flow-electrode capacitive deionization using an aqueous electrolyte with a high Ssalt concentration, Environ. Sci. Technol. 50 (2016) 5892-5899.
[25] P. Nativ, Y. Badash, Y. Gendel, New insights into the mechanism of flow-electrode capacitive deionization, Electrochem. Commun. 76 (2017) 24-28.
[26] X. Xu, M. Wang, Y. Liu, Ting Lu, L. Pan, Ultrahigh desalinization performance of asymmetric flow-electrode capacitive deionization device with an improved operation voltage of 1.8 V, ACS Sustain. Chem. Eng. 5(2017) 189-195.
[27] S. Porada, D. Weingarth, H.V.M. Hamelers, M. Bryjak, V. Presser, P.M. Biesheuvel, Carbon flow electrodes for continuous operation of capacitive deionization and capacitive mixing energy generation, J. Mater. Chem. A 2 (2014) 9313.
[28] S.-i. Jeon, J.-g. Yeo, S. Yang, J. Choi, D.K. Kim, Ion storage and energy recovery of a flow-electrode capacitive deionization process, J. Mater. Chem. A 2 (2014) 6378.
[29] J. Zhang, L. Tang, W. Tang, Y. Zhong, K. Luo, M. Duan, W. Xing, J. Liang, Removal and recovery of phosphorus from low-strength wastewaters by flow-electrode capacitive deionization, Sep. Purif. Technol., in press, https://doi.org/10.1016/j.seppur.2019.116322.
[30] Y. Cho, C.Y. Yoo, S.W. Lee, H. Yoon, K.S. Lee, S. Yang, D.K. Kim, Flow-electrode capacitive deionization with highly enhanced salt removal performance utilizing high-aspect ratio functionalized carbon nanotubes, Water Res. 151 (2019) 252-259.
[31] H. Park, J. Choi, S. Yang, S.J. Kwak, S. Jeon, M.H. Han, D.K. Kim, Surface-modified spherical activated carbon for high carbon loading and its desalting performance in flow-electrode capacitive deionization, RSC Advances 6(2016) 69720-69727
[32] Y. Cho, K.S. Lee, S. Yang, J. Choi, H.-r. Park, D.K. Kim, A novel three-dimensional desalination system utilizing honeycomb-shaped lattice structures for flow-electrode capacitive deionization, Energy Environ. Sci. 10 (2017) 1746-1750.
[33] J. Ma, C. He, D. He, C. Zhang, T.D. Waite, Analysis of capacitive and electrodialytic contributions

to water desalination by flow-electrode CDI, Water Res. 144 (2018) 296-303.
[34] Y. Zhao, Y. Wang, R. Wang, Y. Wu, S. Xu, J. Wang, Performance comparison and energy consumption analysis of capacitive deionization and membrane capacitive deionization processes, Desalination 324 (2013) 127-133.
[35] C. Zhang, D. He, J. Ma, W. Tang, T.D. Waite, Comparison of faradaic reactions in flow-through and flow-by capacitive deionization (CDI) systems, Electrochim. Acta 299 (2019) 727-735.
[36] Y. Gendel, A.K.E. Rommerskirchen, O. David, M. Wessling, Batch mode and continuous desalination of water using flowing carbon deionization (FCDI) technology, Electrochem. Commun. 46 (2014) 152-156.
[37] J.-H. Choi, Comparison of constant voltage (CV) and constant current (CC) operation in the membrane capacitive deionisation process, Desalin. Water Treat. 56 (2014) 921-928.
[38] K.B. Hatzell, M.C. Hatzell, K.M. Cook, M. Boota, G.M. Housel, A. McBride, E.C. Kumbur, Y. Gogotsi, Effect of oxidation of carbon material on suspension electrodes for flow electrode capacitive deionization, Environ. Sci. Technol. 49 (2015) 3040-3047.
[39] K. Tang, S. Yiacoumi, Y. Li, C. Tsouris, Enhanced water desalination by increasing the electroconductivity of carbon powders for high-performance flow-electrode capacitive deionization, ACS Sustain. Chem. Eng. 7 (2018) 1085-1094.
[40] S. Tian, J. Wu, X. Zhang, K. Ostrikov, Z. Zhang, Capacitive deionization with nitrogen-doped highly ordered mesoporous carbon electrodes, Chem. Eng. J. 380 (2020) 122514.
[41] C. He, J. Ma, C. Zhang, J. Song, T.D. Waite, Short-circuited closed-cycle operation of flow-electrode CDI for brackish water softening, Environ. Sci. Technol. 52 (2018) 9350-9360.
[42] K. Fang, H. Gong, W. He, F. Peng, C. He, K. Wang, Recovering ammonia from municipal wastewater by flow-electrode capacitive deionization, Chem. Eng. J. 348 (2018) 301-309.
[43] J. Ma, D. He, W. Tang, P. Kovalsky, C. He, C. Zhang, T.D. Waite, Development of redox-active flow electrodes for high-performance capacitive deionization, Environ. Sci. Technol. 50 (2016) 13495-13501.
[44] S. Yang, H. Kim, S.-i. Jeon, J. Choi, J.-g. Yeo, H.-r. Park, J. Jin, D.K. Kim, Analysis of the desalting performance of flow-electrode capacitive deionization under short-circuited closed cycle operation, Desalination 424 (2017) 110-121.
[45] C. Zhang, J. Ma, T.D. Waite, Ammonia-rich solution production from wastewaters using chemical-free flow-electrode capacitive deionization, ACS Sustainable Chem. Eng. 7 (2019) 6480-6485.
[46] C. Zhang, D. He, J. Ma, W. Tang, T.D. Waite, Faradaic reactions in capacitive deionization (CDI) - problems and possibilities: A review, Water Res. 128 (2018) 314-330.
[47] W. Tang, D. He, C. Zhang, P. Kovalsky, T.D. Waite, Comparison of Faradaic reactions in capacitive deionization (CDI) and membrane capacitive deionization (MCDI) water treatment processes, Water Res. 120 (2017) 229-237.